Backward emitted high-energy neutrons in hard reactions of p and π^+ on carbon

A. Malki,[1] J. Alster,[1] G. Asryan,[2,3] Y. Averichev,[4] D. Barton,[3] V. Baturin,[5,6] N. Bukhtoyarova,[3,6] A. Carroll,[3] S. Heppelmann,[5] T. Kawabata,[7] A. Leksanov,[5] Y. Makdisi,[3] E. Minina,[5] I. Navon,[1] H. Nicholson,[8] A. Ogawa,[5] Yu. Panebratsev,[4] E. Piasetzky,[1] A. Schetkovsky,[5,6] S. Shimanskiy,[4] A. Tang,[9] J. W. Watson,[9] H. Yoshida,[7] and D. Zhalov[5]

[1]*School of Physics and Astronomy, Sackler Faculty of Exact Sciences, Tel Aviv University, Ramat Aviv 69978, Israel*

[2]*Yerevan Physics Institute, Yerevan 375036, Armenia*

[3]*Collider-Accelerator Department, Brookhaven National Laboratory, Upton, New York 11973*

[4]*JINR, Dubna, Moscow RU-141980, Russia*

[5]*Physics Department, Pennsylvania State University, University Park, Pennsylvania 16801*

[6]*Petersburg Nuclear Physics Institute, Gatchina, St. Petersburg RU-188350, Russia*

[7]*Department of Physics, Kyoto University, Sakyoku, Kyoto 606-8502, Japan*

[8]*Department of Physics, Mount Holyoke College, South Hadley, Massachusetts 01075*

[9]*Department of Physics, Kent State University, Kent, Ohio 44242*

(Received 12 March 2001; published 12 December 2001)

Beams of protons and pions of 5.9 GeV/c were incident on a C target. Neutrons emitted into the backward hemisphere, in the laboratory system, were detected in (triple) coincidence with two emerging particles of tranverse momenta $p_t > 0.6$ GeV/c. We determined that for $(46.5 \pm 3.7)\%$ of the proton-induced events and for $(40.8 \pm 4.5)\%$ of the pion-induced events with the two high-p_t particles, there is also at least one backward emitted neutron with momentum greater than 0.32 GeV/c. This observation is in sharp contrast to a well-established universal pattern from a large variety of earlier inclusive measurements with hadrons, electrons, photons, neutrinos, and antineutrinos where the probability for backward nucleon emission was in the 5 to 10 % range. We present also a measurement of the momentum spectra for the backward going neutrons. The spectra have the same universal shape observed in the inclusive reactions. We speculate that the enhanced backward neutron emission in this semi-inclusive region could be an indication for a strong dependence of the cross section on the squared total center-of-mass energy (s) and for the importance of short-range nucleon-nucleon correlations.

DOI: 10.1103/PhysRevC.65.015207 PACS number(s): 21.30.−x, 24.50.+g

I. INTRODUCTION

In this paper we describe a triple-coincidence measurement with 5.9 GeV/c beams and a spectrometer (EVA) that was constructed to measure quasielastic scattering of protons and pions from nuclei near 90° c.m. Neutrons emitted into the backward hemisphere, in the laboratory system, were detected in triple coincidence with two emerging high transverse-momentum (p_t) particles. This experiment was performed at the AGS accelerator at Brookhaven National Laboratory.

This experiment couples the dynamics of high-energy large-momentum-transfer reactions (called hard reactions) with low-energy properties of the nuclear ground state. Until recently almost all nuclear-structure experiments were done with low-energy probes and at low momentum transfer. Almost all hard reaction studies were limited to free hadrons (or very light nuclei such as the deuteron). We present in this introduction a brief description of the kinematics of hard scattering, a scaling law, and the dynamical dependence of the hadron-nucleon cross sections on the relevant observables. We also include a brief description of hadron quasielastic scattering off a bound nucleon in the nuclear medium, and the present status of experiments probing nucleon-nucleon short-range correlations (*NN* SRC) in nuclei. Details can be found in the references. We describe the experimental setup in Sec. II, and the data analysis in Sec. III. We present the results in Sec. IV followed by discussions and conclusions in Sec. V.

The phenomenology of hadronic interactions is often divided into hard and soft interactions. Hard phenomena are characterized by high energy and large momentum transfers (>0.5 GeV/c), which in turn imply that the interaction takes place over a distance which is small with respect to the size of the nucleon. Soft phenomena refer to those reactions for which the energy and momentum transfers are small ($\ll 0.5$ GeV/c). We will focus on two specific hard hadronic interactions: the high-energy large-angle $pp \rightarrow pp$ and $\pi p \rightarrow \pi p$ elastic scattering. See Fig. 1 for pp elastic scattering kinematics. At $\theta_{\mathrm{c.m.}} = 90°$ for a 5.9 GeV/c proton beam we have $E_1 = E_2 = 3.45$ GeV, $p_1 = p_2 = 3.32$ GeV/c, $\theta_1 = \theta_2 = 27.52°$, and $p_{t_1} = p_{t_2} = 1.53$ GeV/c. For most wide-angle

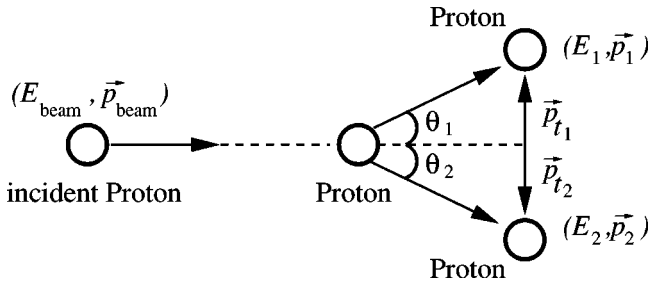

FIG. 1. Kinematics for pp elastic scattering. In quasielastic scattering the target proton in the nucleus has momentum.

exclusive reactions, at incoming momenta above a few GeV/c and $\theta_{\text{c.m.}} > 40°$, the differential cross section scales [1–3] as

$$\frac{d\sigma}{dt}_{AB\to CD} \sim s^{-(n_A+n_B+n_C+n_D-2)} f\left(\frac{t}{s}\right), \tag{1}$$

where n_A, n_B, n_C, and n_D are the number of valence quarks inside the hadrons A, B, C, and D, respectively. For example, $d\sigma/dt_{pp\to pp} \sim s^{-10}$ and $d\sigma/dt_{\pi p\to \pi p} \sim s^{-8}$. The variables s and t are the Mandelstam variables

$$s=(P_A+P_B)^2, \quad t=(P_A-P_C)^2, \tag{2}$$

where P_A, P_B, and P_C are the four-momenta of hadrons A, B, and C, respectively. [Note, that a constant value of t/s in Eq. (1) is equivalent to a constant value of the center of mass scattering angle]. Equation (1), which is known as the dimensional counting rule, was first derived in 1973 [1] in asymptotic form ($s\to\infty, t/s$ fixed), using dimensional analysis. The counting rule is already applicable at $p_{\text{lab}} = 5$ GeV/c [3]. Hendry noted in 1974 [4] that a finer examination of the data reveals small oscillations around Eq. (1). For a review on wide-angle processes see Ref. [5].

In quasielastic (QE) scattering, a projectile scatters from a single bound ''target'' nucleon in the nucleus, while the rest of the nucleus acts as a spectator, and the target nucleon has momentum (Fig. 1). A clear interpretation of QE measurements is possible in the impulse approximation (IA). Within this approximation, it is possible to separate nuclear properties from the reaction mechanism and to study both. In QE scattering, the missing energy (E_m) and momentum ($\vec{p}_m$) are given by $E_m = E_{beam} + m - E_1 - E_2$ and $\vec{p}_m = \vec{p}_{beam} - \vec{p}_1 - \vec{p}_2$. Here, m is the proton mass and the other variables are defined in Fig. 1. In the IA, these observables are associated with the energy E_i and the momentum $\vec{p}_i$ of the target nucleon in the nucleus.

A majority of the QE experiments dealing with nuclear ground state properties have used the $(e,e'p)$ reaction. The $(p,2p)$ reaction is different in interesting ways. The elementary pp cross section is larger than the elementary ep cross section and radiative corrections are negligible compared to electron scattering. On the other hand, the larger pp cross section enhances the role of initial- and final-state interactions. As pointed out by Farrar *et al.* [6], the $(p,2p)$ process provides a powerful amplification of the large longitudinal momentum tails because of the strong energy dependence of pp elastic scattering. The fundamental subprocess of the $(p,2p)$ quasielastic interaction is pp elastic scattering. In the kinematic region of this experiment the energy dependence of pp elastic scattering varies approximately as $1/s^{10}$. Because the cross section greatly favors lower c.m. energies, a target nucleon in the nucleus moving in the direction of the incident beam is expected to have an enhanced probability of contributing to this process [6,7]. The hard-scattering mechanism thus tends to select a nucleon from the nuclear wave function with an anomalously large and positive longitudinal momentum, typically at or above the Fermi momentum. As a result, the pair of high-p_t final-state protons carries away extra positive longitudinal momentum. That extra momentum boost is provided by the nucleus. The residual nucleus or nuclear fragments must recoil backward to balance this extra momentum.

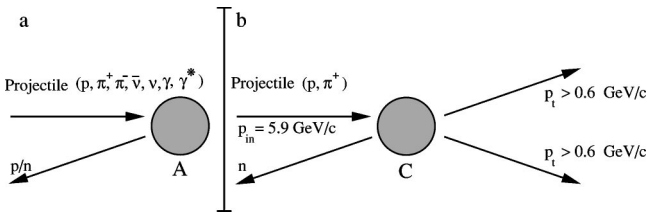

FIG. 2. (a) Schematic of inclusive backward emitted nucleon experiments; γ^* denotes virtual photons. (b) This experiment.

If the struck proton in the nucleus were accelerated to high momentum $\vec{p}_i$ by the mean field of the nucleus, then the recoil would most naturally involve the recoil of the spectator nucleus as a whole [8,9] and would be difficult to observe. On the other hand, if the high-momentum component were associated with a short-range correlation between a proton and a neutron [10,11], then one would expect most of the recoil momentum to be carried away by the correlated neutron partner, see Ref. [12].

The correlated neutron should leave the nucleus after its partner has been scattered away, perhaps retaining the original large momentum and direction. Realizing that for quasielastic processes near 90° c.m. the observable positive-momentum tail of the nuclear momentum distribution is amplified by a large factor, we configured the EVA detector to measure also the associated backward neutron distribution in coincidence with our trigger for two high-p_t particles.

For a broad range of inclusive experiments with high energy (>1 GeV) hadrons [13–16], real photons [17], virtual photons [13], neutrinos and antineutrinos [18–21] a remarkable universality has been observed in the pattern of backward nucleon emission. In those experiments [see Fig. 2(a)] the nucleons were emitted into angles larger than 90° in the laboratory system. The region of backward emission is defined such that it cannot be populated kinematically by interactions between the beam projectile and a single nucleon at rest. These events require the participation of two or more nucleons in the nucleus. Only backward nucleons were taken into account whose momenta were large enough to exclude most low-energy nucleons that ''boil off'' from an excited nucleus. Lower-energy backward emitted neutron data are also in the literature [22].

A common universal form for the momentum spectrum of the backward particles from inclusive reactions was observed, and can be parametrized with the expression

$$(E/p)\frac{d\sigma}{d(p^2)} = Ce^{-B(\theta)p^2} = C'e^{-T/T_0(\theta)}, \tag{3}$$

where E, p, and θ are the energy momentum and angle of the backward-going nucleon B, T_0 are the slope parameters, and C, C' are scale parameters. For incident beams above approximately 1 GeV/c and for backward-emitted nucleons

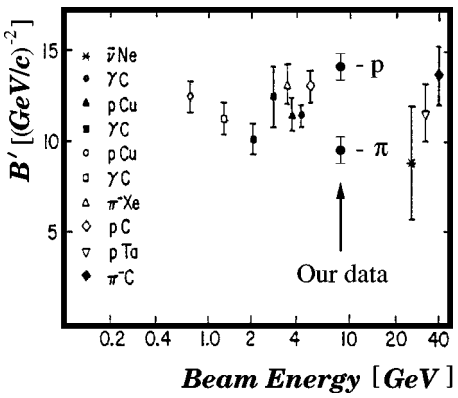

FIG. 3. Comparison of the parameter $B'(120°<\theta<150°)$ obtained for different reactions for various energies and targets. The figure is from Ref. [18]. The arrow indicates our new data points which will be discussed below.

above about 0.3 GeV/c, the slope parameters (B and T_0) were found to be almost independent of incident energy, beam type, and target nucleus.

The neutrino measurements [18–21] report a value of $B=9.5-10.7$ $(\mathrm{GeV}/c)^{-2}$ for protons emitted into the whole backward hemisphere, with uncertainties ranging from 0.3 to 2 $(\mathrm{GeV}/c)^{-2}$. Reference [18] presents a compilation of other experiments at several different energies of hadron and photon beams incident on a variety of targets, including C and other nuclei. For scattered particles into the common angular range of $120°-150°$ of the different experiments, the slope parameters are within the range of $B'=10-12.5$ $(\mathrm{GeV}/c)^{-2}$ with a typical error of 2 $(\mathrm{GeV}/c)^{-2}$ (see Fig. 3). Note that B is used when integrating over the full backward hemisphere, and B' is used for the integration between 120° and 150°.

The universality extends not only to the momentum spectrum but also to the backward-emission rate. The measured invariant momentum spectra for some of the published data were integrated to obtain the total yield of the backward-emitted particles. The yields were then divided by the total inelastic cross section to obtain the *fraction* which is associated with a backward-going particle. The results are presented in Table I.

To summarize the backward neutron-emission data, for a broad range of inclusive experiments there is an almost-constant fraction of events that produce a nucleon at a laboratory angle greater than 90°, and with momentum greater

TABLE I. Backward emission fraction for inclusive reactions.

Incident/ backward emitted particle	Energy (GeV)	Target	Integration range (GeV/c)	Integration range (deg.)	Ref.	Backward fraction (%)
$\bar{\nu}/p$	[a]	Ne	0.2–0.7	90–180	[b1]	7 ± 1
p/p	3.66	Ne	0.2–0.7	90–180	[b2]	8 ± 3
$\bar{\nu}/p$	[c]	Ne	0.2–0.8	90–180	[d]	10 ± 1
ν/p						12 ± 4
NC/p						10 ± 1
$\bar{\nu}/p$	[c]	Ne	0.35–0.8	90–180	[e]	6.0 ± 0.2
ν/p						8.5 ± 0.3
ν/p	[f]	C	0.35–0.7	90–180	[g]	4.45 ± 0.05
p/p	0.64	C	0.311–0.54	90–180	[h]	6.0 ± 1.5
p/n	7.5	C	0.32–0.5	90–180	[i, k]	16
					[j, k]	7.5

[a] A wide band $\bar{\nu}$ beam from 300 GeV/c incident protons [18].

[b1] Results of Ref. [18].

[b2] Deduced in Ref. [18] from measurements of Ref. [14] to satisfy the same selection criteria as used in Ref. [18].

[c] A wide band $\bar{\nu}$ beam from 400 GeV/c incident protons Ref. [19]. NC denotes neutral currents.

[d] From Table I of Ref. [19].

[e] "1 Backward proton rate" from Table I of Ref. [20].

[f] A wide band $\bar{\nu}$ beam from 450 GeV/c incident protons Ref. [21].

[g] From Table 5 of Ref. [21].

[h] Integral of $I(\theta_3)$ from Table 2 of Ref. [16] divided by the total pC inelastic cross section σ_t from Ref. [16].

[i] Data of Ref. [14] for $\theta_n=88°$, see text for details.

[j] Same as *i* for $\theta_n=119°$.

[k] The data of Ref. [14] were integrated between $p_n=0.32-0.5$ GeV/c for $\theta_n=88°$ and $\theta_n=119°$. Assuming that the cross section is constant beyond $\theta_n=88°$ or $\theta_n=119°$, one gets for the full backward hemisphere the results in the table. Since the data show that the cross sections fall with θ_n, these are upper limits. The total inelastic cross section was not given in Ref. [14], thus we estimated it at $(240\pm30$ mb) with a Glauber calculation Ref. [23].

than about 0.3 GeV/c. For light nuclei such as C or Ne, that fraction is about $(10\pm5)\%$. The stability of the universal observation with respect to changes in experimental conditions is remarkable. As the beam energies vary from 1 to 100 GeV the multiplicity of inclusive particle production changes substantially but the fraction of backward nucleons is unchanged. Especially interesting is the observation that even the disruption of a nucleus with neutrinos [18–20], where there is a greatly reduced secondary interaction with spectator nucleons, yields the same universal result.

These results have led to several theoretical interpretations. The models that have been discussed can be divided into two main classes. The models of the first class [8–10,24] deduce from the universality that the measurement must provide direct information on the nuclear ground state, especially on the high-momentum part of the wave function. These models assume that the projectile interacts with a single nucleon and that the backward yield of nucleons is due to the breakup of preexisting clusters of two, or more, correlated nucleons [10,24]. We will discuss below, in more detail, the two-nucleon short-range correlation (*NN* SRC) model. One of the more extreme models in this class assumes that the high momentum of the struck nucleon is balanced coherently by the residual nucleus [8,9]. A second class of models [16,25] assumes that the backward yield is due to rescattering in the nucleus of the incident and outgoing particles. These initial and final interactions include true π absorption and Δ rescattering in the intermediate states. Reference [16] presents detailed comparisons of the inclusive $p+\mathrm{C}\rightarrow p+X$ data with different calculations. The conclusion was that given the uncertainty in the data and the calculations, both the rescattering and the correlation mechanisms are capable of describing the data.

We measured backward-going neutrons in a restricted region of kinematics for proton-carbon or pion-carbon scattering, and found that the probability for backward neutron emission is dramatically larger than the ''universal'' pattern. Our measurements cover a small kinematic region of the inclusive proton-carbon or pion-carbon cross section that we will refer to as in the ''kinematic vicinity of hard quasielastic scattering'' at 90° c.m. Specifically with a proton beam, this kinematic region is loosely characterized by the observation of two high-p_t positively-charged final-state particles that carry away most of the beam energy. The two tracks are observed at large laboratory polar angles, back-to-back in the proton-proton (pp) c.m. frame, within a narrow range of laboratory angles near 90° c.m. The surprising result is that for proton-carbon and pion-carbon scattering in the ''kinematic vicinity of quasielastic hard scattering'' at 90° c.m., the probability for backward neutron emission is greater than 40% in comparison to the universal inclusive result of less than 10%. We point out that we are looking at only a small fraction of the total inclusive cross section.

The backward-emitted neutron data have been interpreted as being due to nuclear correlations [10,24]. The purpose of the present, more exclusive, experiment is to add additional information on this subject. We therefore will end this general introduction by giving a short description of recent measurements of nuclear correlations in nuclei.

Many basic nuclear properties can be described successfully within the single-particle model. However, this simple model breaks down when detailed features are studied, especially in the extreme regions of the nuclear wave function. In recent years much attention has been paid to the importance of *NN* correlations and, specifically, *NN* SRC [26]. The SRC between two nucleons in nuclei are a very elusive feature. Their experimental identification is very difficult because they are small compared to the single-particle components. It is also difficult to separate SRC from other competing processes that can imitate the small expected signal of *NN* SRC. We will mention some experiments that addressed this issue. For the description of electron-scattering experiments we will use the conventional kinematical variables, where Q^2 is the four-momentum transfer, and x is the Bjorken scaling variable.

For inclusive (e,e') experiments [27,28] at high momentum transfers and $x>1$, the extracted momentum distributions for nucleons in the nucleus have relatively large high-momentum tails. Some theoretical models try to explain this by invoking SRC [29]. Others [30] explained the results in terms of final-state interactions (FSI). There are also (e,e') measurements in the ''dip'' region, between the quasielastic peak and the delta region at $x\leqslant1$, which show an anomalously large transverse cross section. This has been cited (see Refs. [31,32] and references in [32]) as evidence for *NN* correlations, although not necessarily of *short* range.

Some $(e,e'p)$ experiments [33–37] observed a depletion of spectroscopic strength by as much as 35% [26]. This has been explained [32,38] by invoking nuclear correlations which push the nucleons to higher-momentum states and high missing energies, and are thus not visible at low momenta and low excitation energies. Other $(e,e'p)$ experiments [39–41], also at $x<1$, show peaks at missing energies corresponding to the removal of two nucleons. Two-nucleon knockout $(e,e'd)$ was also reported recently [42].

In a new generation of ''kinematically complete'' experiments, the knocked out nucleon was measured in coincidence with a correlated nucleon. This category includes $(e,e'pp)$ measurements from MAMI and NIKHEF [43–51], and (γ,NN) from TAGX and LEGS [52,53]. The new virtual-photon measurements identified the shells from which the proton pair was knocked out and studied the contribution of *NN* SRC. Recent calculations [54,55] related those correlations to central (Jastrow type [56]) and tensor components. We point out that the published, kinematically complete, $(e,e'pp)$ measurements are related to virtual photons absorbed on a pp pair. A simple counting of the number of *NN* pairs and the spin-isospin states in the nucleus, produces more *np* than pp pairs. This leads to the expectation that pn pairs will contribute more to the SRC than pp pairs [10].

Next we recall the backward nucleon emission associated with scattering from nuclear targets that we discussed above. As we mentioned, the universal emission pattern of nucleons with momenta large enough to exclude ''boil off'' from an excited nucleus, has been interpreted as indication of SRC in nuclei [10,24].

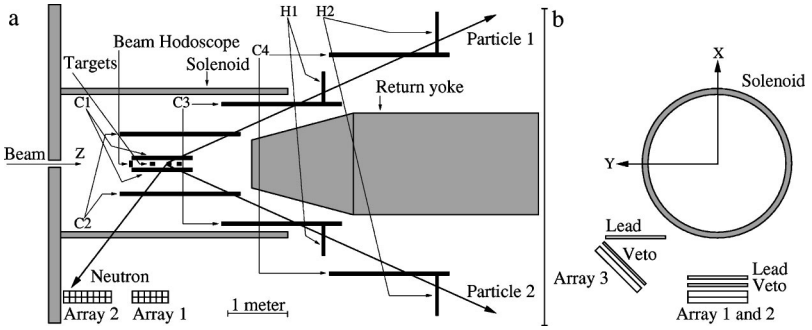

FIG. 4. A schematic side view (a) and a head-on view (b) of the EVA spectrometer and the neutron counter arrays.

There are measurements of backward-scattered protons from $(e,e'p)$ experiments at $x \leqslant 1$ [57] and deep-inelastic $(\nu,\mu p)$ [20] scattering, where backward-going protons were observed in coincidence with a forward-going particle, electron and muon, respectively. Correlations were claimed between the transferred energies and the momenta of the backward-going protons. Preliminary results for events with a forward-scattered electron in coincidence with a backward-emitted proton indicate a sensitivity of the scattered electron spectra to the backward-proton momentum and angle [58]. This is as expected from SRC dominance.

Finally, we mention a triple-coincidence experiment at BNL which studied the quasielastic $(p,2p)$ reaction in coincidence with a neutron with momentum above the nuclear Fermi momentum k_F. A correlation between the direction of the missing momentum and the emitted-neutron momentum was found [11]. The simplest explanation of this experimental observation relates it to the dominance of *NN* SRC.

To summarize this introduction, there is evidence for large-momentum tails of nucleons in nuclei, for general two-nucleon (not necessarily short range) correlations, and evidence for SRC (not necessarily two nucleon). We emphasize the word ''short'' in SRC in order to distinguish them clearly from correlations which could be either short or long range. The two-nucleon emphasis in *NN* correlations is in order to distinguish them from possible multinucleon correlations. Since the early theoretical work of Jastrow [56] there is a continuing theoretical effort [10,29,59–62] to confront the SRC picture with experimental data. There is an overall consensus about the importance of *NN* SRC, but a satisfactory quantitative description is still missing.

In this paper we present the results of a measurement of high-energy backward neutrons emitted from a nucleus in coincidence with two high-p_t particles. Beams of protons and pions of 5.9 GeV/c were incident on a C target. Neutrons emitted into the backward hemisphere in the laboratory system were detected in (triple) coincidence with two emerging $p_t > 0.6$ GeV/c particles, as shown in Fig. 2(b). The cross section for this process is a very small fraction of the inclusive cross section for the same beams, but larger than the quasielastic cross section. We will put forward the hypothesis that *NN* SRC is the dominant aspect of our selected events and that it could be possible, with some theoretical input, to obtain quantitative information on the contribution of two-nucleon SRC to the large-momentum nucleon tail in nuclei.

II. EXPERIMENTAL SETUP

A. Beam, beam detectors and the EVA spectrometer

We present results from a measurement which was performed during 1998 with the rebuilt EVA spectrometer at the AGS accelerator of Brookhaven National Laboratory. The spectrometer consisted of a superconducting solenoidal magnet 2 m in diameter and 3.35 m long, operated at 0.8 T (see Fig. 4).

The scattered particles were tracked by four sets of four-layer straw-tube drift chambers ($C1$–$C4$ in Fig. 4 and Table II). The cylindrical chambers were arranged concentrically around the beam axis. The straw tubes were made of spirally wrapped, aluminum-clad Mylar. They operated with a gaseous mixture of ethane (50%) and argon (50%) at slightly above atmospheric pressure, with positive high voltage on the central resistive wire, and the interior aluminum cladding at ground. The resistive wire enabled the determination of the hit position along the wire via the charge division of the pulses at both ends of the wire.

The straw tubes measured the three coordinates of points along charged tracks with varying precision. High-precision determination of the transverse coordinates of points were required to measure the transverse projection of tracks in the longitudinal magnetic field. They provide the p_t and the charge of the outgoing particle. The polar scattering angles were determined from the longitudinal coordinates of track hits by (lower-precision) straw-tube charge division.

Two sets of fan-shaped scintillator hodoscopes, each with 2π acceptance [see Fig. 4(a)], provided an online fast trigger. The first hodoscope $H1$, was located just downstream from the magnet, and had 256 elements, thus measuring the azimuthal angle of a track to an accuracy of ± 12 mr at an average radius of about 1.3 m. The second hodoscope $H2$ was positioned around the downstream edge of $C4$, and consisted of 256 overlapping counters, providing 512 azimuthal

TABLE II. Physical parameters of the four straw-tube chambers.

Chamber	Inner radius	Length	Number of tubes	Diameter of tubes
$C1$	10 cm	100 cm	512	0.5 cm
$C2$	45 cm	200 cm	1024	1.0 cm
$C3$	90 cm	200 cm	2048	1.0 cm
$C4$	180 cm	200 cm	2048	2.0 cm

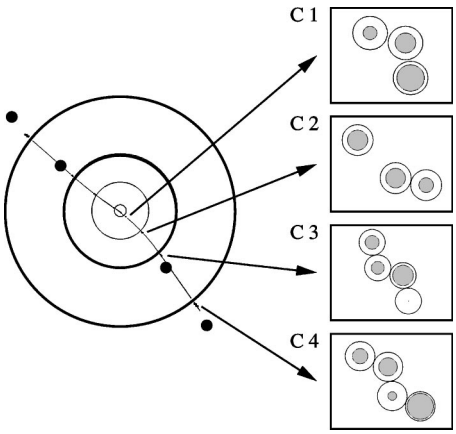

FIG. 5. A two-track event in EVA, projected on the plane transverse to the beam. The small dots are hits in the chambers ($C1-C4$). The big dots represent hits in the $H1$, $H2$ hodoscopes. The figures on the right are blow-ups of the hits in the cylinders. The circles and the shaded areas represent the tube sizes and the drift distances, respectively.

sections with an azimuthal angle accuracy of ± 6 mr at an average radius of 2 m. A typical event with two tracks of positively charged particles in EVA is shown in Fig. 5.

Details on the EVA spectrometer straw-tube system are given in Refs. [63–66]. For this run the spectrometer was upgraded with the installation of two new neutron-counter arrays, which increased the acceptance for backward neutrons by a factor of 2.5 over the configuration in Ref. [11]. See Sec. II B for details.

At a momentum of 5.9 GeV/c, the beam consisted of about 40% protons and 60% pions, which were identified by a sequence of two differential Cerenkov counters. The beam entered along the symmetry axis (z) of the magnet with an intensity of $\approx 1\times 10^7$ particles over a one-second spill, every 3 sec. A four-finger scintillator hodoscope, located upstream of the spectrometer, served as the timing reference for neutron time-of-flight measurements. Three solid targets consisting of various combinations of CH_2 and C were placed on the z axis, separated by about 20 cm. The targets were 5.1 $\times 5.1$ cm^2 wide and 6.6 cm long in the z direction. Their positions were interchanged several times at regular intervals. Some of the runs used three C targets and some used two C targets and one CH_2 target.

We triggered the spectrometer on two positively charged particles which emerged from the downstream end of the solenoid at polar angles of $(27.5\pm 3)°$ (around 90° in the pp c.m.). The polar-angle coverage of the inner straw-tube cylinder extended from about 10° to 150°. The major role of the trigger system is to select high-p_t events and to exclude the more abundant low-p_t events. We used three levels of triggering. The scintillator hodoscopes $H1$, $H2$ provided fast triggering for the first level, by requiring a hit pattern (a maximum angle between the hits in $H1$ and the $H2$ counters) that selected p_t above a threshold. The second-level trigger used input from the straw tubes to require at least one track with a higher-momentum threshold. The third-level software trigger required two tracks, one to the left of the beam and the other to the right, in addition to a low multiplicity of hits in the straw tubes. See Ref. [66] for a detailed description of the trigger system. For a typical run with 1×10^7 particles per spill and three carbon targets, the overall trigger rate was about 70 triggers/sec, and the ''live time'' was about 60%.

B. Neutron detectors

Three scintillator arrays measured the direction and energy of neutrons in coincidence with the two high-p_t particles required in the trigger. In Fig. 4 we show the relative position of the EVA spectrometer and the neutron-detector arrays. The first array of 12 scintillator bars (array 1 in Fig. 4) was placed below the targets covering an area of 0.6 $\times 1.0$ m^2 and 0.25 m (2 layers 0.125 m each) deep. This array spanned a polar angular range of 84° to 110°, and an azimuthal range from 165° to 195°. A second double-layer array of 16 scintillator bars (array 2), covering an area of 0.8×1.0 m^2 and 0.25 m deep, spanned a polar angular range of 110° to 132° and the same azimuthal range as the first one. Each individual detector in these two arrays was 10 $\times 12.5\times 100$ cm^3 in size, and had a 5.1 cm photomultiplier at each end. The third array (array 3) was constructed from one layer of eight $10\times 25\times 100$ cm^3 detectors with a 12.7 cm photomultiplier at each end. This third array covered an area of 2.0×1.0 m^2 and spanned a polar angular range of 72° to 120° and an azimuthal range from 120° to 150°. A set of veto counters covered with 1.7 radiation length lead sheets, shown in Fig. 4(b) only, served to discriminate against charged particles and photons converted in the lead.

We set all neutron detectors to an electron-equivalent detection threshold of 1 MeV, by fixing a discriminator level at the Compton edge of a ^{60}Co gamma source. This procedure is similar to the description in Ref. [67]. We calculated the detection efficiency by the Monte Carlo method described in Ref. [68]. The efficiencies depend on the neutron momentum, and they ranged from about 30% at 0.15 GeV/c to about 15% at 0.5 GeV/c, for a typical single detector. We considered only neutrons above 0.15 GeV/c to avoid large uncertainties in the efficiency calculations of the neutrons at low momenta. We calculated the fraction of the neutrons lost to absorption along their trajectory from the target to the detectors by assuming that the removal cross section was equal to the nonelastic cross sections in the materials [69]. We assigned an uncertainty of 25% to these removal cross sections. The attenuation values ranged from about 35% at the low momenta to about 20% at the high momenta. This translates to an approximate overall normalization error of 6% in the absolute neutron yields.

Neutron momenta were determined from their times of flight (TOF). A clearly identified peak due to photons from the targets was used for calibration and to measure the timing resolution. That time resolution was $\sigma\leqslant 1$ ns, which corresponded to a momentum resolution of $\sigma=30$ MeV/c at the highest momentum (0.5 GeV/c). We applied a cut in the TOF spectrum at 7 ns/m, keeping neutrons below 0.5 GeV/c, in order to eliminate the photons that were not converted in the lead.

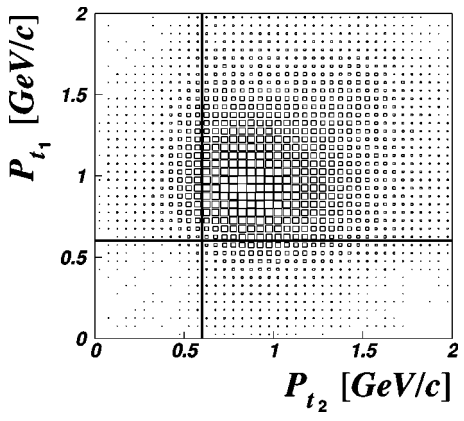

FIG. 6. The measured distribution of p_{t_1} versus p_{t_2} for the two charged tracks. The solid lines indicate the cuts made at $p_t > 0.6$ GeV/c.

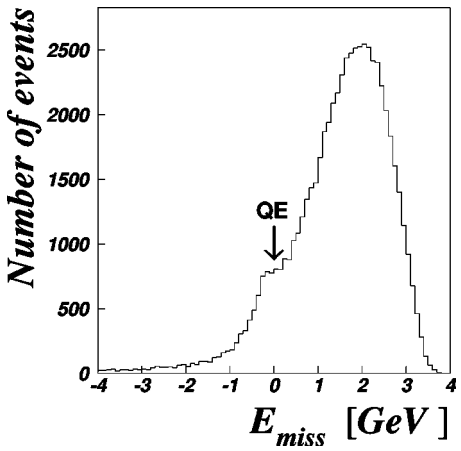

FIG. 7. The missing-energy spectrum for the selected events with both $p_t > 0.6$ GeV/c.

III. DATA ANALYSIS

The definition of the class of events that we described as lying in the ''kinematic vicinity of quasielastic hard scattering'' involves the detection of two positively-charged tracks with $p_t > 0.6$ GeV/c with a vertex that points to one of the C targets. The tracks must have polar angles within the trigger acceptance $(27.5 \pm 3)°$. We required that there be no additional charged tracks in the straw chambers in the polar angular range from about 10° to 150°. We also required good-quality track reconstruction and consistent Cerenkov-detector beam identification. We will refer to Y_2 as the yield of these selected events. About 3% of the triggers satisfied these conditions and only about 5% of those Y_2 events registered a hit in the neutron detectors.

Our measurement is semi-inclusive. The events that satisfy the above-mentioned criteria are not all the result of purely quasielastic scattering. While we know that we do not observe any extra charged tracks over a large part of the laboratory solid angle, we have no information about possible charged tracks in the very forward or backward directions. We also know little about neutral-particle production beyond the detected neutrons.

Figure 6 shows the distribution of the p_{t_1} versus the p_{t_2} where p_{t_1} is for the charged particle with the smaller polar angle, and p_{t_2} is for the particle with the larger polar angle. A missing-energy spectrum for the events with both $p_t > 0.6$ GeV/c, as indicated by the solid lines in the figure, is shown in Fig. 7. In a typical selected event there are two particles, each with a p_t of about 0.8 to 1.0 GeV/c and a typical missing energy which is less than about 2 GeV in the laboratory frame (1 GeV in the c.m. frame). This restricts kinematically the number of particles that can be produced together with the main two high-p_t charged particles.

IV. RESULTS

A. Invariant momentum spectra

Guided by Eq. (3), we present in Fig. 8 the measured invariant neutron-momentum spectra $(E_n/p_n) \times dY_3/Y_2 d(p_n^2)$ (in arbitrary units) for pion and proton incident beams, where E_n and p_n are the energy and momentum of the neutron detected in the backward hemisphere $(90° < \theta_n < 130°)$. The effective yield of triple-coincidence events which fulfills all the conditions of the Y_2 events and, in addition, have a single neutron in the scintillator bars, is indicated by Y_3. The effective yield Y_3 includes event-by-event corrections to efficiency and attenuation which both depend on the neutron momentum. The uncertainties introduced by these corrections were discussed in Sec. II. We plotted the resulting spectra on a semilogarithmic scale as a function of p_n^2. The error bars represent the statistical errors only. We fitted the data above $p_n^2 > 0.1$ $(\mathrm{GeV}/c)^2$ to a first-order polynomial. The slope parameters [B in Eq. (3)] for the proton and pion incident beams are shown in Fig. 8 with their fitting errors.

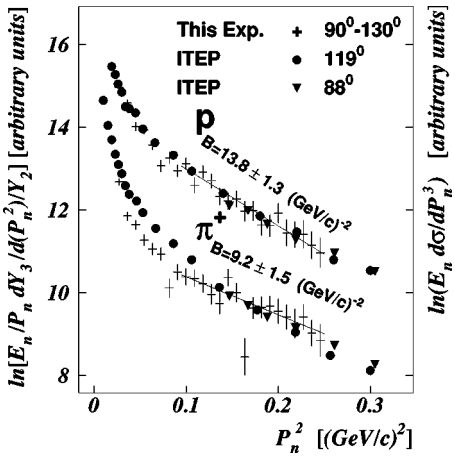

FIG. 8. Proton and pion induced neutron invariant momentum spectra. The vertical axis is $\ln[(E_n/p_n) \times dY_3/Y_2 d(p_n^2)]$. The horizontal axis is p_n^2. E_n and p_n are the energy and momentum of the neutron. Y_2 and Y_3 are the double and triple coincidence yields defined in the text. Above $p_n^2 > 0.1$ $(\mathrm{GeV}/c)^2$ the points are fitted to a straight line to obtain the slope parameter defined in Eq. (3). The resulting slopes with the fitting errors are shown. ITEP stands for data from Ref. [15] for which the right-hand scale applies.

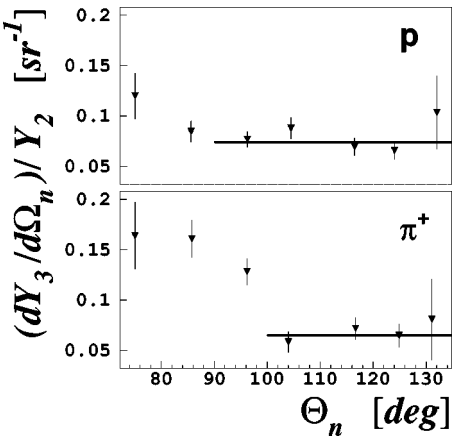

FIG. 9. The relative yield per unit solid angle $dY_3/Y_2 d\Omega_n$ of neutrons above 0.32 GeV/c as a function of the neutron angle. Y_3 and Y_2 are the same as in Fig. 8. The data are for the proton and pion induced reactions. The lines represent fits to constants [(7.4 ± 0.4)%/sr for protons and (6.5 ± 0.6)%/sr for pions) which are used to estimate the total backward-emission yield, see text.

For comparison, we show in Fig. 8 inclusive data from Ref. [15] for $p+\mathrm{C} \rightarrow n+X$ and $\pi^- + \mathrm{C} \rightarrow n+X$, for kinematics similar to those of our data. We labeled these data ''ITEP,'' and renormalized them for comparison with our results. The slope parameter reported in Ref. [15] for the $p+\mathrm{C} \rightarrow n+X$ data at 7.5 GeV/c and 119° is $B=13.0 \pm 0.8$ $(\mathrm{GeV}/c)^{-2}$. We recall that the neutrino measurements [18–20] report a value of $B=9.5$–10.7 $(\mathrm{GeV}/c)^{-2}$ for protons emitted into the whole backward hemisphere with uncertainties ranging from 0.3 to 2 $(\mathrm{GeV}/c)^{-2}$. Reference [18] presents a compilation of other experiments at several different energies for hadron and photon beams incident on a variety of targets, including C and other nuclei. For particles in the common angular range of 120°–150° for the different experiments, the slope parameters all lie within the range of 10–12.5 $(\mathrm{GeV}/c)^{-2}$ with a typical error of 2 $(\mathrm{GeV}/c)^{-2}$ (see Fig. 8). The slopes measured in this experiment fit the universal pattern within the measured uncertainties. The angular ranges are not the same for all experiments but this does not modify the values of B sufficiently to affect this conclusion (see Ref. [20]). Note that although the slopes for our data, and the ''ITEP'' data in Fig. 8 are very similar, the *yields* are very different, as discussed in the next section.

B. Yield of backward emitted neutrons

We compare our yield of backward-scattered neutrons above 0.32 GeV/c to those from the other experiments. In Fig. 9 we show the triple-coincidence yield Y_3 per unit solid angle divided by the double-coincidence yield Y_2 yield vs the neutron angle. We corrected Y_3 for neutron detection efficiency and attenuation, event-by-event, depending on the neutron energy and direction. The errors in the figure are the statistical errors, combined with up to 10% systematic errors due to software cuts, and uncertainties in the neutron detection thresholds. Of the data presented in Fig. 9, we will concern ourselves only with the data for angles above 90°. At smaller angles the neutrons can originate from direct reactions and not necessarily from two-nucleon correlations. Also, we wish to compare our data to the earlier inclusive neutron-production measurements for the backward hemisphere.

To obtain the relative yield into the backward hemisphere, we fitted the ratios $dY_3/Y_2 d\Omega_n$ for the proton and pion induced reactions to a constant above 90° and 100°, respectively, where the ratios become constant (see Fig. 9). This procedure produces integrated neutron yields $(90° - 130°)$ per selected event of (29.9 ± 2.4)% and (26.2 ± 2.9)% for the proton and pion induced reactions, respectively. These errors include the overall normalization error.

These relative yields need to be compared to those of the inclusive measurements mentioned in the introduction [16,18,19], which were integrated over angles from 90° to 180°. Those inclusive measurements found yields between 6 and 9%. We note that even though our data extend only to 130°, we obtain much larger ratios. If we use the parameters of the fits for the backward angles to extrapolate to $\theta_n = 180°$, assuming that the ratios remain constant, the integrated yields increase to (46.5 ± 3.7)% and (40.8 ± 4.5)% for the proton and pion induced reactions, respectively.

We note that our data have no additional charged tracks in the angular acceptance of the chambers. If we relax this condition and allow one or more additional charged tracks, in order to become ''more inclusive,'' the probability of neutrons for angles below of 90° increases by 30–50 % while the backward neutron production is not significantly changed.

V. SUMMARY AND CONCLUSIONS

We observed the same shape for the momentum distribution for backward-emitted neutrons as was found in earlier inclusive measurements. Our significant observation is that for events in the ''kinematic vicinity of quasielastic hard scattering'' near 90° c.m. proton-carbon or pion-carbon quasielastic scattering, nearly 1/2 of the events produced a backward neutron with momentum greater than 0.32 GeV/c. This probability is more than four times greater than the universally observed probability for various inclusive interactions. A pattern of universality without an explanation is an opportunity for new discovery. Sometimes it is the ''exception'' to the rule that can suggest the underlying mechanism.

There are no models in the literature that have considered an increase in the backward neutron production for events in the ''kinematic vicinity'' of quasielastic scattering. However models that attempt to explain the universal inclusive results do exist. One approach [16,25] proposes that the source of backward-emitted nucleons is initial-state or final-state rescattering from spectator nucleons of particles associated with the primary interaction. We are not aware of any features of the kinematic regime of our measurements which would cause a large enhancement of rescattered backward neutrons above that of other kinematic topologies.

The other approach [10,24] is the one discussed in the intoduction to this paper, namely, that the backward-neutron enhancement may be associated with *NN* correlations. We suggest that a strong *s* dependence in the cross section can be

associated with events in the kinematic region of our measurement. This would imply that the consequences of short-range correlations are enhanced by large energies and momentum transfers. The correlation picture is closely related to an interpretation that we suggested for the triple-coincidence measurement in the quasielastic region for the reaction $^{12}C(p,2p+n)$ [11] and with a forthcoming paper of a recent measurement of the same reaction [70].

We hypothesize that the large probability for backward-neutron emission in this semi-inclusive region indicates a strong dependence in the cross section on the total c.m. energy (s), and the dominance of *NN* SRC. However, in addition to *NN* SRC, there can be other sources for production of high-energy backward neutrons such as intial-state and final-state interactions, and mean-field effects. We indicated that the contributions of these competing processes are small but they should be calculated in order to extract from our measurement a quantitative statement about the contribution of two-nucleon SRC to the large momenta of nucleons in the nucleus. Such a calculation is beyond the scope of this experimental paper. We hope that the intriguing data we present here will encourage such a calculation, and thus provide a novel quantitative understanding of SRC.

In the introduction to this paper we mentioned the extensive set of data from $(e,e'N)$ and $(e,e'NN)$ reactions as a source for detailed information on SRC. So far the published triple-coincidence data are for $(e,e'pp)$ which is related to *pp* SRC in nuclei. The data presented in this paper, within the interpretation we offer, are related to *np* SRC pairs. One expects that *np* pairs will contribute more to the large nucleon momenta in nuclei than *pp* pairs. A unified theoretical framework that will compare and confront our data with the electromagnetic measurements is desirable, but clearly not available yet. We hope these data, together with results from new proposed measurements, will lead to such theoretical approach.

ACKNOWLEDGMENTS

We wish to thank Drs. L. Frankfurt, M. Strikman, and M. Sargsian for their theoretical input. We are pleased to acknowledge the assistance of the AGS staff in building and rebuilding the detector and supporting the experiment, particularly our liaison engineer C. Pearson. We acknowledge the continuing support of Drs. D. Lowenstein and P. Pile. This research was supported by the U.S.–Israel Binational Science foundation, the Israel Science Foundation founded by the Israel Academy of Sciences and Humanities, NSF Grants No. PHY-9501114, PHY-9722519, and the U.S. Department of Energy Grant No. DEFG0290ER40553.

[1] S.J. Brodsky and G.R. Farrar, Phys. Rev. Lett. **31**, 1153 (1973); V.A. Matveev, R.M. Muradyan, and A.N. Tavkhelidze, Lett. Nuovo Cimento Soc. Ital. Fis. **7**, 719 (1973).
[2] G.P. Lepage and S.J. Brodsky, Phys. Rev. D **22**, 2157 (1980).
[3] P.V. Landshoff and J.C. Polkinghorne, Phys. Lett. **44B**, 293 (1973), and references therein.
[4] A.W. Hendry, Phys. Rev. D **10**, 2300 (1974).
[5] D. Sivers *et al.*, Phys. Rep. **23**, 1 (1976).
[6] G.R. Farrar, H. Liu, L.L. Frankfurt, and M.I. Strikman, Phys. Rev. Lett. **62**, 1095 (1989).
[7] Y. Mardor *et al.*, Phys. Lett. B **437**, 257 (1998).
[8] S. Frankel, Phys. Rev. Lett. **38**, 1338 (1977).
[9] R.D. Amado and R.M. Woloshyn, Phys. Rev. Lett. **36**, 1435 (1976).
[10] L.L. Frankfurt and M.I. Strikman, Phys. Rep. **76**, 215 (1981); **160**, 235 (1988).
[11] J. Aclander *et al.*, Phys. Lett. B **453**, 211 (1999).
[12] A. de Shalit and H. Feshbach, *Theoretical Nuclear Physics* (Wiley, New York, 1974).
[13] G. A. Lesin (unpublished).
[14] Yu.D. Bayukov, L.S. Vorob'ev, G.A. Lesin, V.L. Stolin, V.B. Fedorov, and V.D. Khovanskii, Sov. J. Nucl. Phys. **18**, 639 (1974); Yu.D. Bayukov *et al.*, *ibid.* **42**, 116 (1985); **42**, 238 (1985); **34**, 437 (1981).
[15] Yu.D. Bayukov *et al.*, Sov. J. Nucl. Phys. **41**, 101 (1985); ITEP-5-1985 (unpublished).
[16] V.I. Komarov, G.E. Kosarev, H. Müller, D. Netzband, V.D. Toneev, T. Stiehler, S. Tesch, K.K. Gudima, and S.G. Mashnik, Nucl. Phys. **A326**, 297 (1979).
[17] K.V. Alanakyan, M.Dzh. Amaryan, R.A. Demirchyan, K.Sh. Egiyan, M.S. Ogandzhanyan, and Yu.G. Sharabyan, Sov. J. Nucl. Phys. **25**, 292 (1977).
[18] J.P. Berge *et al.*, Phys. Rev. D **18**, 1367 (1978).
[19] V.I. Efremenko *et al.*, Phys. Rev. D **22**, 2581 (1980).
[20] E. Matsinos *et al.*, Z. Phys. C **44**, 79 (1989).
[21] P. Astier *et al.*, Nucl. Phys. **B609**, 255 (2001).
[22] M.R. Adams *et al.*, Phys. Rev. Lett. **74**, 5198 (1995).
[23] M. Zhalov (private communication).
[24] L.L. Frankfurt and M.I. Strikman, Phys. Lett. **69B**, 93 (1977).
[25] V.B. Kopeliovich, Sov. J. Nucl. Phys. **26**, 87 (1977).
[26] V.R. Pandharipande, I. Sick, and P.K.A. deWitt Huberts, Rev. Mod. Phys. **69**, 981 (1997).
[27] D.B. Day *et al.*, Phys. Rev. Lett. **59**, 427 (1987).
[28] J. Arrington *et al.*, Phys. Rev. Lett. **82**, 2056 (1999).
[29] L.L. Frankfurt, M.I. Strikman, D.B. Day, and M. Sargsyan, Phys. Rev. C **48**, 2451 (1993).
[30] O. Benhar and V.R. Pandharipande, Phys. Rev. C **47**, 2218 (1993).
[31] J.S. O'Connell *et al.*, Phys. Rev. Lett. **53**, 1627 (1984); Phys. Rev. C **35**, 1063 (1987).
[32] W. Bertozzi, R. W. Lourie, and E. J. Moniz, in *Modern Topics in Electron Scattering*, edited by B. Frois and I. Sick (World Scientific, Singapore, 1991).
[33] P.E. Ulmer *et al.*, Phys. Rev. Lett. **59**, 2259 (1987).
[34] J.H. Koch and N. Ohtsuka, Nucl. Phys. **A435**, 765 (1985).
[35] G. van der Steenhoven, H.P. Blok, E. Jans, L. Lapikas, E.N.M. Quint, and P.K.A. De Witt Huberts, Nucl. Phys. **A484**, 445 (1988).
[36] L. Lapikás, G. van der Steenhoven, L. Frankfurt, M. Strikman, and M. Zhalov, Phys. Rev. C **61**, 064325 (2000).

[37] J. Gao *et al.*, Phys. Rev. Lett. **84**, 3265 (2000).
[38] L. Frankfurt, M. Strikman, and M. Zhalov, Phys. Lett. B **503**, 73 (2001).
[39] J.M. Le Goff *et al.*, Phys. Rev. C **50**, 2278 (1994).
[40] C. Marchand *et al.*, Phys. Rev. Lett. **60**, 1703 (1988).
[41] J.J. van Leeuwe *et al.*, Nucl. Phys. **A631**, 593c (1998).
[42] R. Ent *et al.*, Phys. Rev. Lett. **62**, 24 (1989).
[43] C.J.G. Onderwater *et al.*, Phys. Rev. Lett. **78**, 4893 (1997).
[44] L.J.H.M. Kester *et al.*, Phys. Rev. Lett. **74**, 1712 (1995).
[45] A. Zondervan *et al.*, Nucl. Phys. **A587**, 697 (1995).
[46] C.J.G. Onderwater *et al.*, Phys. Rev. Lett. **81**, 2213 (1998).
[47] R. Starink *et al.*, Phys. Lett. B **474**, 33 (2000).
[48] D.L. Groep *et al.*, Phys. Rev. Lett. **83**, 5443 (1999).
[49] D.L. Groep *et al.*, Phys. Rev. C **63**, 014005 (2000).
[50] K.I. Blomqvist *et al.*, Phys. Lett. B **421**, 71 (1998).
[51] G. Rosner, Prog. Part. Nucl. Phys. **44**, 99 (2000).
[52] J. Arends, J. Eyink, H. Hartmann, A. Hegerath, B. Mecking, G. Nöldeke, and H. Rost, Z. Phys. A **298**, 103 (1980).
[53] M. Kanazawa, S. Homma, M. Koike, Y. Murata, H. Okuno, F. Soga, N. Yoshikawa, and A. Sasaki, Phys. Rev. C **35**, 1828 (1987).
[54] J. Ryckebusch, S. Janssen, W. Van Nespen, and D. Debruyne, Phys. Rev. C **61**, 021603(R) (2000).
[55] S. Janssen, J. Ryckebusch, W. Van Nespen, and D. Debruyne, Nucl. Phys. **A672**, 285 (2000).
[56] R. Jastrow, Phys. Rev. **98**, 1479 (1955).
[57] K.V. Alanakyan *et al.*, Phys. At. Nucl. **61**, 207 (1998).
[58] K. Egiyan *et al.*, Bull. Am. Phys. Soc. **45**, 32 (2000).
[59] C. Ciofi Degli Atti and G.B. West, Phys. Lett. B **458**, 447 (1999).
[60] J. M. Laget, in *New Vistas in Electronuclear Physics*, edited by E. Tomusiak *et al.* (Plenum, New York, 1986).
[61] V. Van der Sluys, J. Ryckebusch, and M. Waroquier, Phys. Rev. C **54**, 1322 (1996).
[62] J. Ryckebusch, Phys. Lett. B **383**, 1 (1996).
[63] M. A. Shupe *et al*, EVA, a solenoidal detector for large angle exclusive reactions: Phase I - determining color transparency to 22 GeV/*c*, Experiment E850 Proposal to Brookhaven National Laboratory, A. Carroll, S. Heppelmann, spokespersons, 1988.
[64] S. Durrant, Ph.D. thesis, Pennsylvania State University, 1994.
[65] Y. Mardor, Ph.D. thesis, Tel Aviv University, 1997; I. Mardor, Ph.D. thesis, Tel Aviv University, 1997.
[66] J. Wu, E.D. Minor, J.E. Passaneau, S.F. Heppelmann, Chu. Ng, G. Bunce, and I. Mardor, Nucl. Instrum. Methods Phys. Res. A **349**, 183 (1994).
[67] R. Madey *et al.*, Nucl. Instrum. Methods **214**, 401 (1983).
[68] R.A. Cecil, B.D. Anderson, and R. Madey, Nucl. Instrum. Methods **161**, 439 (1979).
[69] D. J. Hughes and R. B. Schwartz, BNL Report No. 325, 1958.
[70] A. Tang *et al.* (unpublished).